

Bell V-280 Hover Flight Dynamics Model Validation and Update with Flight Test Data

Mark J. S. Lopez
Aerospace Engineer
U.S. Army Combat Capabilities
Development Command
Aviation & Missile Center
Moffett Field, CA, USA

Caitlin S. Duffy
V-280 Control Law Engineer
Bell
Fort Worth, Texas, USA

Mark B. Tischler
Senior Technologist (Retired)¹
U.S. Army Combat Capabilities
Development Command
Aviation & Missile Center
Moffett Field, CA, USA

Paul Ruckel
V-280 Control Law IPT Manager
Bell
Fort Worth, Texas, USA

ABSTRACT

Flight dynamics simulation models are a key tool for enabling modern flight control design; however, advanced configurations such as the Bell V-280 Valor tiltrotor proposed for the U.S. Army Future Long Range Assault Aircraft program require advancements in existing flight dynamics models. This work uses flight test data to validate the accuracy of V-280 flight dynamics models of various levels of fidelity including a low fidelity Froude scale model, a physics based simulation model, and a high fidelity system integration lab. Model fidelity in hover is assessed using system identification including the Joint Input-Output method to extract frequency responses from flight test data and subsequently identify a state space model with respect to individual redundant control effectors. The identification results from flight test data are then used to update a physics-based model comparing two different update approaches: a simple gain and time delay correction versus a more complex force and moment increment correction. The implementation complexity as well as benefits and limitations for both methods are examined for the V-280.

NOTATION

A	State space dynamics/stability matrix	u	Control input (state space notation)
a_x	Longitudinal accelerometer measurement		Body-axis forward velocity
a_y	Lateral accelerometer measurement	v	Body-axis sideward velocity
a_z	Vertical accelerometer measurement	w	Body-axis downward velocity
B	State space input/control matrix	x	Dynamic state
$E_{1,2}$	Error response of 1 with respect to 2	Y	Side force
k	Magnitude gain	y	Output response
L	Roll moment	δ	Control input (generalized input notation)
N	Yaw moment	θ_0	Trim Euler pitch attitude
p	Roll rate		
q	Pitch rate	θ	Euler pitch attitude
r	Yaw rate	τ	Time delay
s	Laplace variable, differentiation operator	ϕ	Euler roll attitude

Presented at the Vertical Flight Society's 77th Annual Forum & Technology Display, Virtual, May 10-14, 2021. Copyright © 2021 by the Vertical Flight Society. All rights reserved.

Distribution Statement A: approved for public release; distribution is unlimited

¹Retired from U.S. Army; Currently Tischler Aeronautics

INTRODUCTION

Accurate flight dynamics models are a key component in the fly-by-wire flight control development process. An initial estimate for flight dynamic predictions can be obtained using empirical techniques such as Froude scaling from a known prior configuration (Ref. 1). While Froude scaling provides a quick initial estimate it is only a rough estimate for gross vehicle dynamics. High-fidelity models can be obtained using physics-based modeling techniques which formulate and connect individual component forces, moments, and kinematics (Ref. 2). While both empirical and physics-based models provide a good initial prediction, there will always be errors in the models due to uncertainties in the input parameters and unmodeled phenomena. Thus, it is important for flight dynamics models to be validated with actual vehicle flight-test data once available, then updated accordingly to improve agreement with flight test data.

Recent work by Berrigan et al. (Refs. 3 and 4) applied frequency-domain system identification techniques (Ref. 5) and the Joint Input-Output (JIO) Method (Ref. 6) to obtain frequency responses from flight test data for the Bell V-280 in hover. Berrigan et al. used the frequency responses to validate the control effectiveness of Bell's V-280 physics-based model. The work in this paper builds on the prior work by validating the full-flight dynamic response in hover for both empirical and physics-based models. After the initial validation assessment, updates to the models were developed to improve agreement with flight test data. Model validation and update methods used herein leveraged the work of the recently completed NATO AVT-296 Research Task Group on Rotorcraft Simulation Model Fidelity Assessment and Update Methods (Ref. 7).

V-280 Flight Testing

The V-280 is Bell's next generation tiltrotor designed for the Future Long-Range Assault Aircraft (FLRAA) program of record. The V-280 is a tiltrotor design, where the two rotors are mounted on pylons which can tilt from a vertical position (Fig. 1) to a horizontal position. The vertical pylon position allows for Vertical Take-Off and Landing (VTOL) flight like a rotorcraft, while the horizontal position allows for cruise like a conventional airplane. The V-280 uses rotor collective and cyclic inputs for VTOL mode control authority, flaperon and ruddervator control surfaces for cruise mode, and a combination of both for conversion regimes (between VTOL and cruise modes).

The individual rotor collective and cyclic controls are mixed, or ganged, together into symmetric and differential combinations to provide virtual effectors in the traditional control axes. Specifically in VTOL mode: symmetric collective (Coll) is the virtual effector which provides thrust control, symmetric longitudinal cyclic (Symm Lon) provides pitch control, differential longitudinal cyclic (Diff Lon) provides directional control, and a combination of

Differential Collective Pitch (DCP) and symmetric lateral cyclic (Lat Cyclic) are the virtual effectors which both provide roll control.



Figure 1. V-280 in VTOL Mode flight.

System identification data were collected on the V-280 in flight test including frequency sweeps and piloted doublets. Frequency sweeps included automated and piloted sweeps from the inceptors (δ_s in the block diagram in Figure 2) as well as virtual effector automated sweeps injected downstream of the mixer ($\delta_{A,m}$ in Figure 2). The combination of automated and piloted sweeps provided the best balance of data quality, test consistency, and minimizing the number of test points (Ref. 3). The combination of stick and effector sweeps allows for frequency responses to be computed with respect to individual virtual effectors. All flight data were collected with the stability augmentation system active (closed loop) but without higher augmentation modes to obtain the best quality flight data (least augmented vehicle response) while still maintaining safety and airworthiness.

Kinematic Consistency and Corrections

Once flight data are collected, the signals are checked for quality and consistency prior to extracting bare-airframe frequency responses (Ref. 5). Ideally frequency responses for attitude rates (e.g. q) and differentiated attitudes (e.g. $s\theta$) would be equal however in practice there is usually some discrepancy in the instrumentation or post processing which should be accounted for. Figure 3 shows the longitudinal kinematic consistency check for pitch rate q versus differentiated pitch attitude $s\theta$. Over nearly the entire frequency range, both responses are nearly equal. There is a small amount of phase lead for $(s)\left(\frac{\theta}{\text{symm lon}}\right)$ at the higher frequency range which can be corrected by adding a small amount of time delay to the pitch attitude θ time responses. The corrections are calculated by identifying a gain k and time delay τ of the inverse of the error response:

$$\frac{1}{E_{s\theta,q}} = \frac{q/\text{symm lon}}{s(\theta/\text{symm lon})} \approx k e^{-s\tau} \quad (1)$$

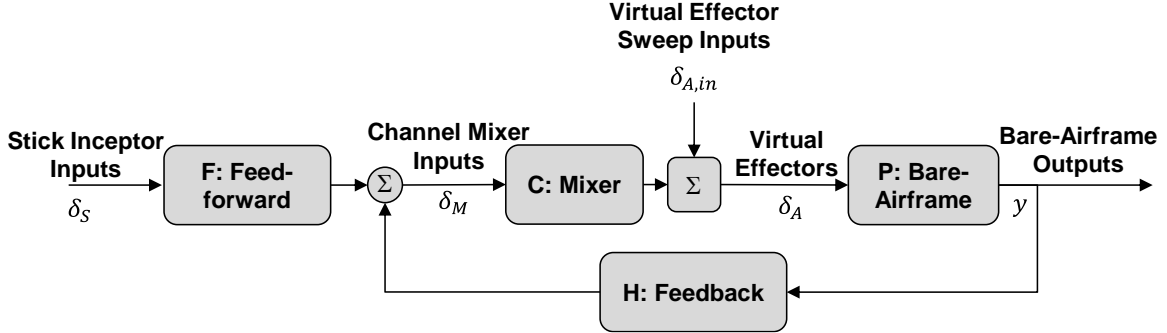


Figure 2. Generalized Closed-Loop Block Diagram.

where $E_{s\theta,q}$ is the error response of $s\theta$ with respect to q , τ is the delay correction for θ , and k is the gain correction for θ (although in this case $k = 1$). Similar results are found for lateral kinematic consistency checks with roll rate p and differentiated roll attitude $s\phi$.

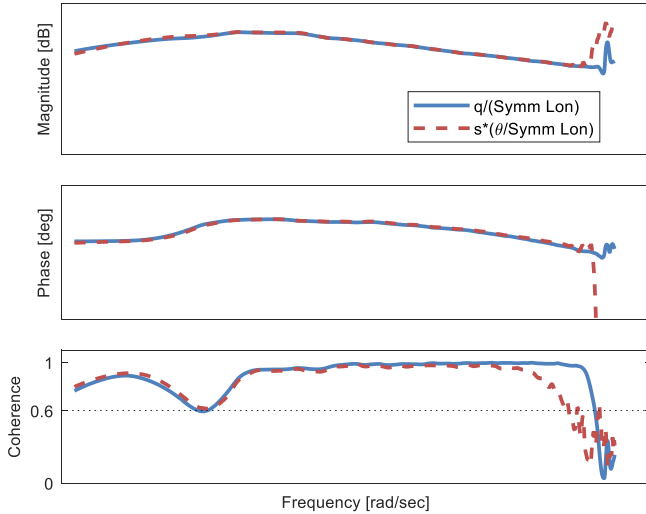


Figure 3. Longitudinal Kinematic Consistency.

FREQUENCY RESPONSE IDENTIFICATION

Once the flight test data have been checked for consistency, they can be used in the bare-airframe frequency response identification process.

Speed Damping Identification

The first frequency response computed is for the identification speed damping derivatives. Low frequency acceleration responses to attitude can help to identify speed damping derivatives which are often difficult to accurately identify from the multi-input-multi-output state space identification procedure due to the required data being located at very low frequency (Ref. 5).

The speed damping derivatives can be identified by assuming that only the speed damping derivative contributes at

sufficiently low frequency, effectively isolating them in the identification procedure. Specifically, the speed damping derivative X_u can be identified from the simplified body x-axis acceleration response to attitude, which is valid at low frequency (Ref. 5):

$$\frac{\dot{u}}{\theta} \approx \frac{-g \cos(\theta_0) s}{s - X_u} \quad (2)$$

where X_u is the longitudinal speed damping derivative of interest. The \dot{u}/θ frequency response and corresponding identified model is shown in Figure 4. The identified model is only valid at the low frequency range for which flight test data is shown. It was found that identifying X_u in this manner provided speed damping that was consistent with expectations (correct sign and rough order of magnitude) which was fixed later in the state space identification process. A similar process for the low-frequency lateral body-axis acceleration response was used to obtain the lateral speed damping derivative Y_v .

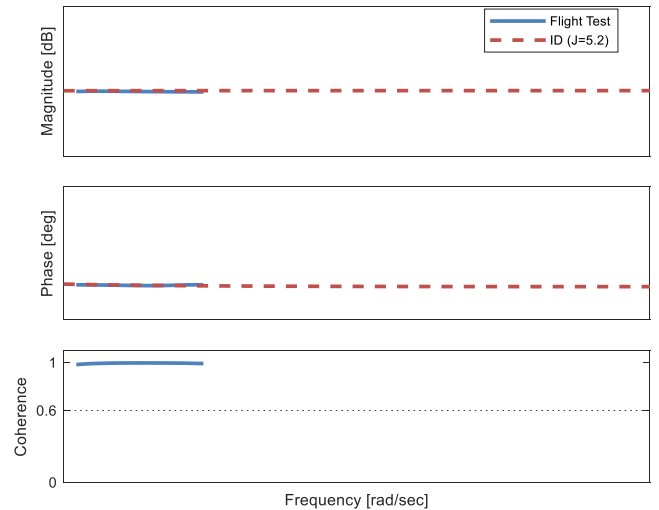


Figure 4. Low Frequency Longitudinal Body-Axis Acceleration Response.

While no specific values (e.g. magnitude, phase, or frequency) are provided due to the sensitive nature of the data,

all frequency response figures presented herein are consistent in scale so that the reader can visually compare responses. Additionally, the frequency range is consistent among all frequency response figures to highlight applicable frequency ranges (e.g. low, med, and high frequency ranges).

Effector Cross-Control Correlation

Prior to identifying the bare airframe responses themselves, the effector-cross-control correlation is evaluated to determine whether a traditional Direct Method (Ref. 5) system identification approach can be used or whether the JIO Method (Ref. 6) should be used instead. Cross-control correlation is determined by identifying the coherence between two control effectors (cross-control coherence) for a given frequency sweep. The Direct Method should be used if controls are at most partially correlated (cross-control coherence is below 0.5 on average) or if secondary control inputs do not significantly contribute to the measured responses; the JIO method should be used if controls are highly correlated (cross-control coherence is above 0.5 on average).

Figure 5 shows the cross-control coherence for a lateral inceptor sweep between the Lateral channel Mixer input (Lat Mixer) and individual virtual effectors: DCP, Lat Cyclic, and Diff Lon. Lat Mixer inputs are geared with DCP and Lat Cyclic, so unsurprisingly the cross-control coherence is 1.0 among all three, and thus indicates that the individual control effectors are fully correlated. Cross-control coherence between Lat Mixer and Diff Lon is slightly lower, but still above 0.5 for the majority of the frequency range shown. The high correlation for each effector indicates that for the lateral inceptor sweep, the Direct Method cannot be used and the JIO method should be used instead.

Figure 6 shows the cross-control coherence for a DCP sweep between the DCP and the other three lateral-directional controls available: Lateral Mixer, Lat Cyclic, and Diff Lon. As has been demonstrated before (Refs. 4 and 8), injecting a sweep to an individual effector still can result in high correlation due to the combination of feedback which rejects the effector input and a mixer which causes the other effectors to respond. This can be seen by cross-control coherence which is high but not perfectly 1.0 (as the case was for a lateral inceptor sweep). Again, the high correlation for each effector indicates that for the DCP sweep, the JIO method should be used.

It is important to point out that the cross-control coherence at low-to-mid frequencies drops below 0.5, which corresponds to the frequency range around the peak of the hovering cubic. This low cross-control coherence directly contributes to the resulting bare-airframe responses computed by the JIO method having poor coherence at the same frequency range around the hovering cubic. This is one of the primary factors for responses computed via the JIO Method generally having acceptable coherence over a smaller frequency range as compared to the Direct method.

Lastly, Figure 7 shows the cross-control coherence for a pedal sweep between the Diff Lon and the other three lateral-directional controls available: DCP, Lat Cyclic, and Lateral Mixer. Interestingly the cross-control coherence from Diff Lon to the other three effectors is below 0.5 for the majority of the frequency range shown. This indicates that the Direct Method can and should be used for computing the Diff Lon responses from pedal sweeps.

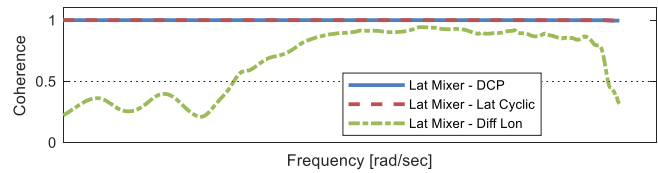


Figure 5. Cross-Control Coherence Lateral Inceptor Sweep.

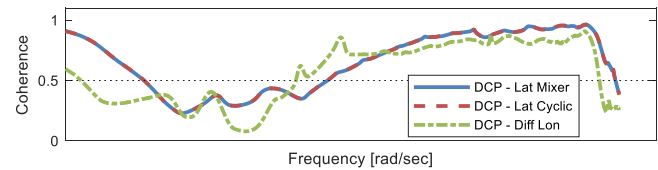


Figure 6. Cross-Control Coherence DCP Sweep.

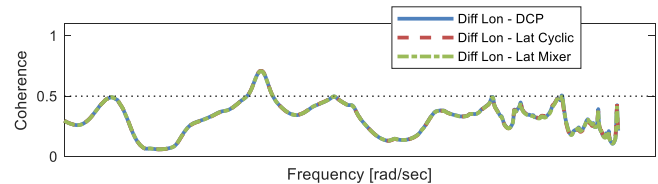


Figure 7. Cross-Control Coherence Pedal Sweep.

Bare Airframe Frequency Responses

Berrigan et al. (Ref. 4) used frequency domain system identification (Ref. 5), in particular the JIO Method (Ref. 6), to extract frequency responses from the V-280 flight test data. Since DCP and Lat Cyclic both provide roll control, in VTOL mode flight they are further ganged to act as a single lateral channel mixer input (Lat Mixer) and thus are always fully correlated. The full correlation of DCP and Lat Cyclic necessitated the application of the JIO method to separate the frequency response contributions of DCP from Lat Cyclic. Berrigan et al. (Ref. 4) focused on extracting frequency responses for DCP and Lat Cyclic to validate control effectiveness. Herein, frequency responses will be extracted using a combination of the Direct Method and the JIO method, leveraging the benefits of both methods where possible.

Frequency responses were extracted for each combination of virtual effectors (Coll, Symm Lon, Diff Lon, DCP, and Lat Cyclic) and vehicle rigid body measurements (rigid body attitudes, rigid body rates, accelerometer, and body-axis accelerations). Sample lateral-directional frequency responses are shown in Figure 8 and Figure 9 where DCP and Lat Cyclic responses are computed using the JIO Method, while Diff Lon responses are computed using the direct method. As expected in hover, the coupling response of p /Diff Lon has a lower coherence indicating lower energy transfer compared to DCP and Lat Cyclic.

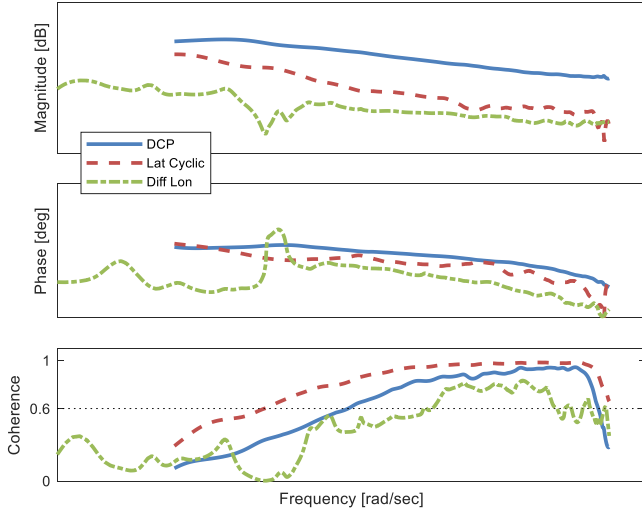


Figure 8. Roll Rate Frequency Response for Various Effectors.

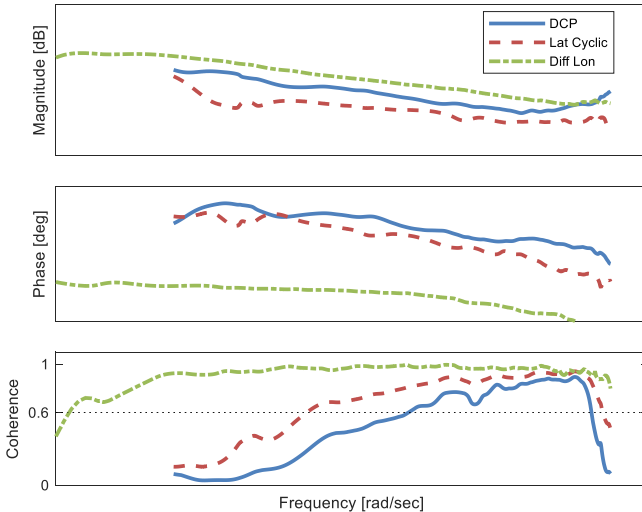


Figure 9. Yaw Rate Frequency Response for Various Effectors.

STATE SPACE IDENTIFICATION

Bare Airframe State Space Identification

The identified frequency responses were used to identify a hover state space model. While the frequency responses to DCP and Lat Cyclic are sufficient for determining control effectiveness, they were extracted using the JIO method with a combination of two data sets: excitations at the pilot stick inceptor (δ_S in Fig. 2), and excitations summed directly into the actuator commands ($\delta_{A,In}$ in Fig. 2). This JIO combination with two data sets is referred to herein as JIO Case A. The excitations summed directly into the actuator commands $\delta_{A,In}$ can result in lower frequency response quality. Specifically, poor quality at low frequency ranges can be observed if frequency sweeps injected directly at the effector commanded are used in JIO (Ref. 8). To address this, frequency responses were also extracted from the lateral channel mixer input Lat Mixer using an extra JIO calculation (referred to herein as JIO Case B) which only uses sweeps at the pilot stick inceptor δ_S and have higher quality overall. Table 1 shows the setups used for JIO Case A and JIO Case B. Note that JIO is still needed to calculate the lateral channel mixer input responses because Diff Lon is highly correlated to Lat Mixer during the lateral stick sweeps due to strong lateral-directional coupling.

The state space identification utilized responses for DCP, Lat Cyclic, and Lat Mixer to provide sufficient data for a full state-space identification. The DCP and Lat Cyclic responses provide sufficient data for identifying control derivatives (high frequency), while the lateral channel mixer input responses provide improved data for identifying stability derivatives (low and mid frequencies). A comparison of the roll rate response to DCP, Lat Cyclic, and lateral channel mixer input is shown in Figure 10. The responses computed from JIO Case A (DCP and Lat Cyclic) have lower response quality as indicated by the lower low-frequency coherence when compared to the JIO Case B (Lat Mixer).

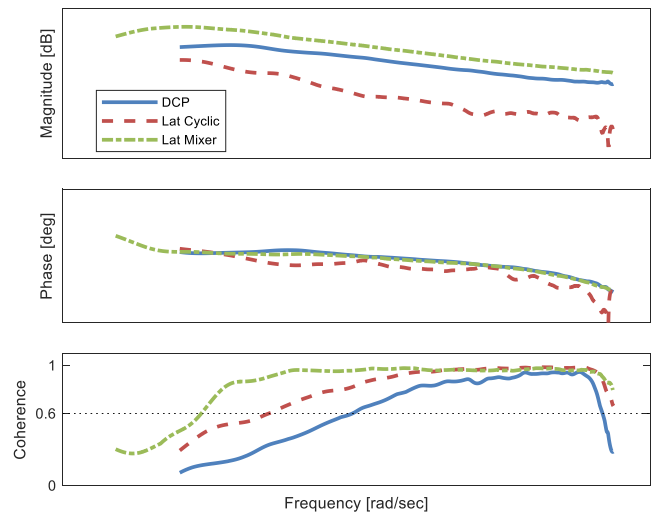


Figure 10. Lateral Input Roll Rate Response Quality Comparison.

Table 1. Setup for JIO

Case	Sweep Types	Identified Effector Responses
JIO Case A	1) Lateral Stick Sweeps	1) DCP
	2) DCP Effector Sweeps	2) Lat Cyclic
	3) Pedal Sweeps	3) Diff Lon
JIO Case B	1) Lateral Stick Sweeps	1) Lat Mixer
	2) Pedal Sweeps	2) Diff Lon

A matrix of all inputs-output pairs used in the state-space identification and the methodology for extracting the corresponding frequency responses (Direct Method or JIO Method) is shown in Table 2. A six degree-of-freedom (6DOF) rigid body state space model was identified. The identified state space model is of the form:

$$\dot{x} = Ax + Bu \quad (3)$$

$$y = Cx + Du \quad (4)$$

where x is the state vector, u is the control input vector, and y is the output measurement vector. Note that only terms in the state equation (3) are identified. The output equation (4) is not directly identified; rather it is based on kinematic constraints which relate the states and state derivatives to the measured outputs (i.e., accelerometer measurement is a function of body axis acceleration and attitude):

$$y = H_0x + H_1\dot{x} \quad (5)$$

The state equation (3) is substituted for the state derivatives in the kinematic output equation (5) resulting in the outputs being a function of states and controls (4), and thus implicitly includes the identified parameters.

All identified parameters were found with satisfactory accuracy: Cramer-Rao bounds $CR_i < 40\%$ and insensitivities $I_i < 20\%$ in accordance with the guidelines of Ref 5. The

average cost function was $J_{ave} = 94 < 100$ indicating an overall acceptable level of fidelity with respect to the flight test data (Ref. 5). Each of the individual frequency responses were also found to have good agreement with the flight test data. The individual cost functions and frequency response comparisons will be illustrated in subsequent sections for brevity.

Time Domain Verification

The identified state space model is validated in the time domain with piloted doublets. The doublets are performed on each inceptor channel (power lever, lateral inceptor, longitudinal inceptor, and pedals). Each doublet is used to validate the corresponding axis for the identified state space model with a dataset dissimilar in character from the original dataset used to identify the model (i.e., doublets are characteristically different from frequency sweeps); this is done to ensure that the model is not over-tuned to match the flight test data used for identification.

The effector inputs for the flight test lateral inceptor doublet response are shown in Figure 11. The effector inputs from flight test data are used to excite the identified model, and the resulting responses are compared with the flight test responses in Figure 12. It can visually be observed that the identified model closely correlates with the measured flight test data. This is corroborated by the excellent time response quantitative assessments of RMS Cost $J_{RMS} = 0.35 < 1$ and Thiel Inequality Coefficient $TIC = 0.06 < 0.35$ (Ref. 5). Similar results were observed for each of the other axes.

Table 2. Matrix of input-output pairs and extraction methodology

	Coll	Symm Lon	DCP	Lat Cyclic	Diff Lon	Lat Mixer
p	-	-	JIO Case A	JIO Case A	Direct	JIO Case B
q	-	Direct	-	-	-	-
r	-	-	JIO Case A	JIO Case A	Direct	JIO Case B
a_x	-	Direct	-	-	-	-
a_y	-	-	JIO Case A	JIO Case A	Direct	JIO Case B
a_z	Direct	Direct	-	-	-	-
udot	-	Direct	-	-	-	-
vdot	-	-	JIO Case A	JIO Case A	Direct	JIO Case B

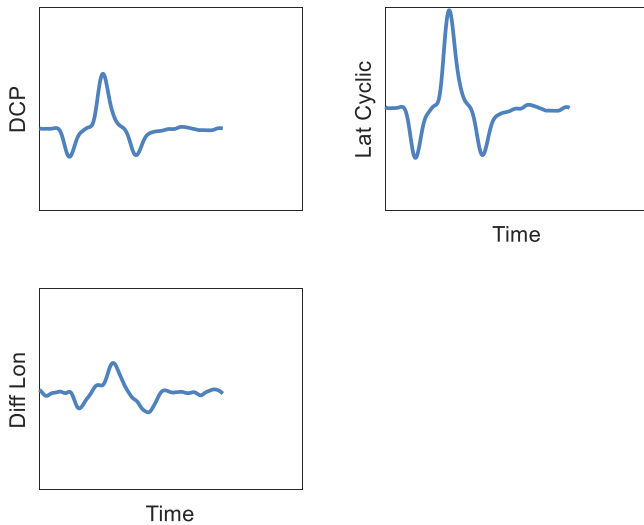


Figure 11. Lateral Incept Doublet, Virtual Effector Inputs.

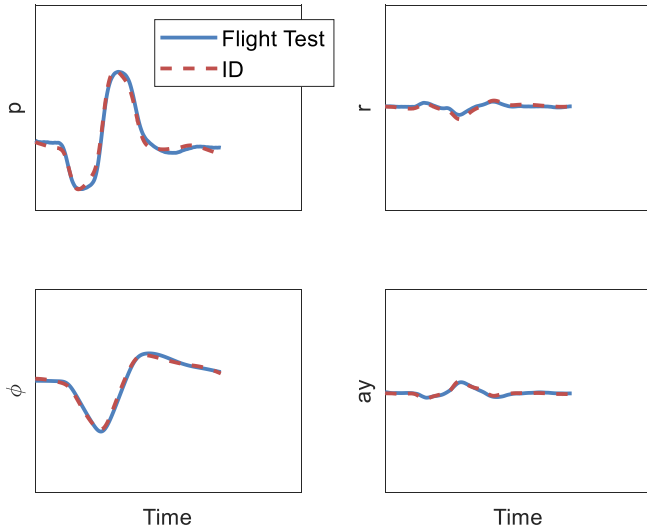


Figure 12. Lateral Inceptor Doublet, Vehicle Responses.

FLIGHT DYNAMICS MODEL VALIDATION

The flight test data identified response can be used to validate flight dynamics models of the aircraft. Flight dynamics models have various levels of fidelity from analytic close form back of the envelope computations to high-fidelity physics based models. Even high-fidelity physics-based models will not perfectly correlate to the flight test data due to uncertainties in the model data as well as assumptions used to create the model itself. Thus, each model should be validated against the flight test data to give confidence to the model predictions.

Froude Scale Model

A quick initial estimate of the V-280 flight dynamics can be obtained by Froude scaling another flight dynamics model, in

this case the Bell XV-15 which was an experimental tiltrotor platform extensively studied in the 1970's. Flight accurate state-space models of the XV-15 have been identified by Tischler and Remple (Ref. 5) and were Froude scaled up to the V-280 size based on the hub-to-hub distance following Ivler et al. (Ref 1). The XV-15, Froude scaled to V-280 size, allows for a quick rough order of magnitude empirical estimation prior to both developing physics-based models and actual flight testing.

It should be noted that there are limitations of using the XV-15 identified model by Tischler and Remple (Ref. 5) as the basis for the Froude scale model. Firstly, the identified model only includes lateral and directional responses; longitudinal and heave responses were not identified and therefore are not included in the XV-15 Froude scale model. Also, for roll-channel control, the XV-15 only used DCP; Lat Cyclic was not used and thus corresponding responses are not available. Lastly, the XV-15 flight data secondary responses to Diff Lon (e.g. $p/\text{Diff Lon}$, $a_y/\text{Diff Lon}$, and $\dot{v}/\text{Diff Lon}$) did not have sufficient coherence and were not included in the state-space identification process; thus while the XV-15 Froude scale model does have non-zero secondary responses to Diff Lon, they are also dropped for XV-15 Froude scale analysis herein.

Physics Based Models

Physics-based models for the V-280 were developed both by Bell and the U.S. Army Combat Capabilities Development Command Aviation & Missile Center (DEVCOM AvMC). The independent models allowed for each organization to do a secondary check on flight dynamics predictions prior to actual flight testing. The Bell model is built using Bell's Generic Tiltrotor (GTR) simulation, which has been previously validated for other Bell tiltrotor platforms. The GTR model provides the bare-airframe characteristics (aerodynamic forces and moments, rotor kinematics, rigid body kinematics) which is one of the key components for the Bell high fidelity System Integration Lab (SIL). The DEVCOM AvMC model is built using HeliUM (Ref. 9), which is a blade-element model developed at the University of Maryland with Army support and has been previously validated against other flight test data and comprehensive simulation models for other configurations.

Model Validation Results

Each of the models can be validated against the flight test data using frequency response comparisons and quantitative assessments. The SIL frequency responses are obtained using system identification. The HeliUM frequency responses are obtained by first linearizing the nonlinear HeliUM model, and then computing frequency responses from the resulting linear model.

The cost function assessment proposed by Tischler (Ref. 5) will be used here to quantitatively assess model fidelity. A cost function $J < 50$ is considered excellent, while a cost function $J < 100$ is considered acceptable. The frequency

response validation along with the associated cost functions for each model are shown in pitch rate response to Symm Lon in Figure 13, roll rate response to DCP in Figure 14, yaw rate response to DCP in Figure 15, and yaw rate response to Diff Lon in Figure 16. For the responses shown, all of the models predict responses which vary in accuracy when compared with the flight test data.

One interesting feature noted is the additional damping of the hovering cubic peak depicted in Figure 13. At low-to-mid frequency, the hovering cubic peak is predicted to be much higher than the actual flight test data indicates. In fact, there is no known linear 6DOF solution that provides the damping observed in the flight test data hovering cubic while still being kinematically consistent with all other responses (as indicated by the ID model which has lower damping compared with the flight test data). This result has been observed before in the XV-15 lateral hovering cubic (Ref. 5) as well as other hovering aircraft.

All of the responses which are both available for the XV-15 and also sufficiently identified for the V-280 are shown herein. This includes the two primary responses p /DCP and r /Diff Lon, and only one secondary response r /DCP. The XV-15 Froude scale model correlates well with the flight test data with respect to the rough fidelity level of Froude scaling.

For the responses shown, the Bell SIL does an exemplary job of correlating with flight test data. The Bell SIL also correlates well with the flight test data for all other responses (including those not shown) with an overall average cost function of $J_{ave}=130$. This is a result of the combined high levels of fidelity for GTR for the bare-airframe as well as the use of the actual flight hardware in the SIL where possible, particularly the sensor measurement system.

The HeliUM model correlates well with flight test data for primary responses, but has poor correlation for secondary responses. This is in part due to deficiencies in the bare-airframe modeling but also low-fidelity approximations for the sensor measurement system. As such, the HeliUM bare airframe model will be the focus for the later section on model updates.

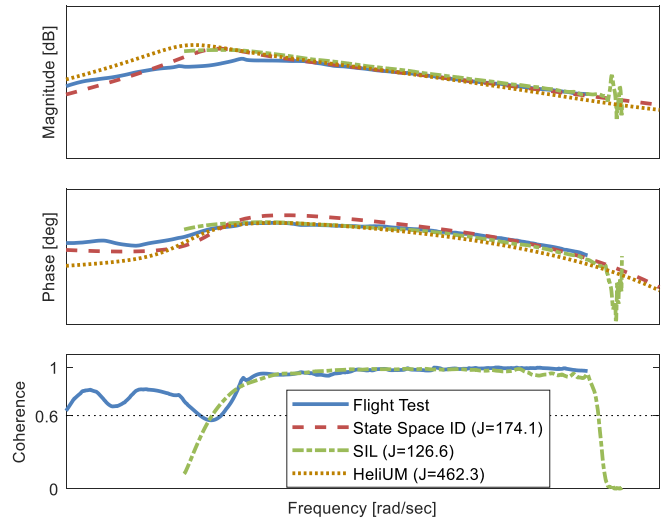


Figure 13. V-280 Pitch Rate Response to Symm Lon Validation.

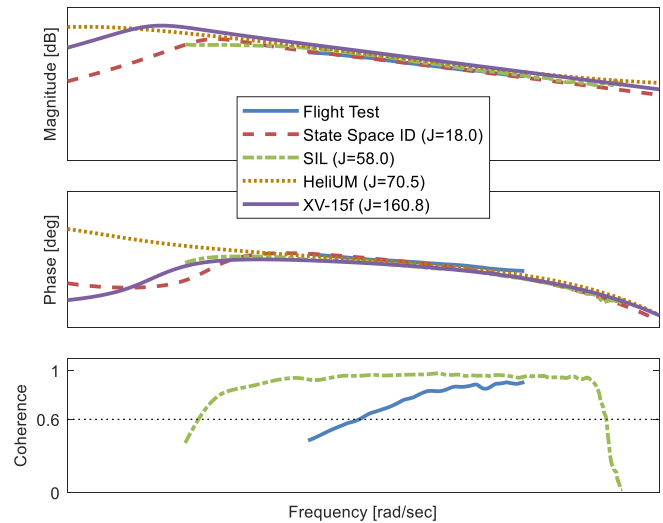


Figure 14. V-280 Roll Rate Response to DCP Validation.

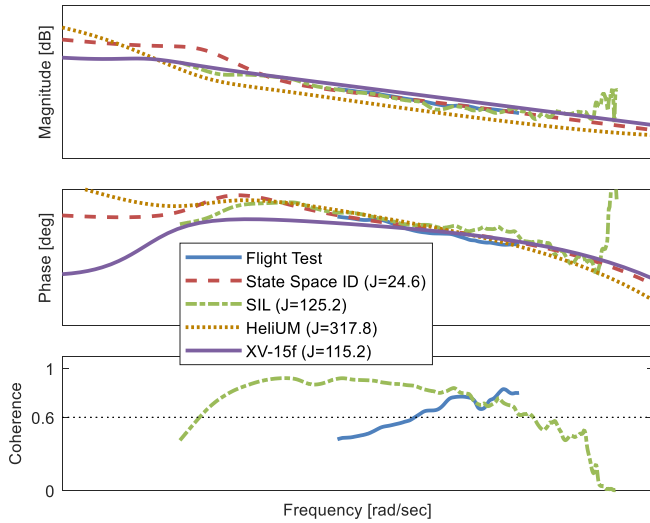


Figure 15. V-280 Yaw Rate Response to DCP Validation.

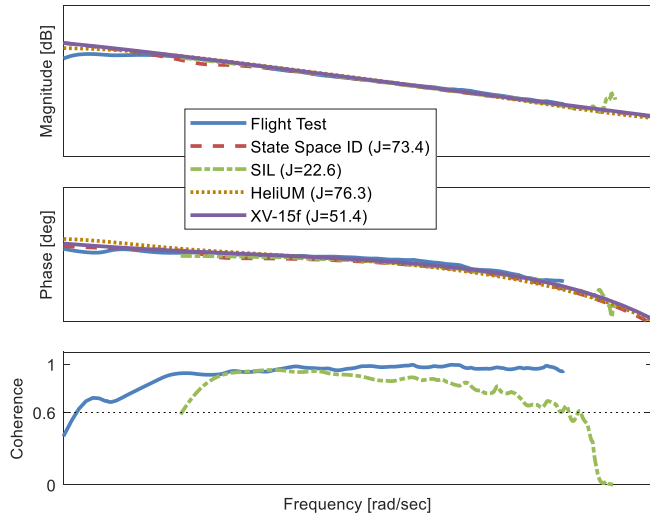


Figure 16. V-280 Yaw Rate Response to Diff Lon Validation.

MODEL UPDATE

While the models have good agreement with flight test data, the correlation is not perfect and can be improved using model update methods. While the identified model itself can be used for updating the flight control design, the model update methods provide additional confidence to the models for cases where the identified model is not directly suitable (i.e., alternate flight/loading condition, in piloted simulation, or analyzing deficiencies in the physics based model). Several model update methods have been demonstrated in the literature and in particular was focus of the recently completed NATO AVT-296 Research Task Group was Rotorcraft Flight Simulation Model Fidelity Improvement and Assessment (Ref. 7). While many update methods exist, two different methods are used here to compare effectiveness of both.

For the work presented herein, the model updates will be presented for the DEVCOM AvMC HeliUM model only; a similar procedure can be used to update the Bell GTR model. The HeliUM nonlinear model can be expressed in explicit ordinary differential equation (ODE) form:

$$\dot{x} = f(x, u; t) \quad (6)$$

where the equations of motion are functions of state x , control input u , and time t . The purpose of the model update procedure is used to improve the fidelity of the nonlinear model (i.e. updates are applied to nonlinear simulation); however it is convenient to analyze the net effects using the resulting linear models from the updated nonlinear simulation.

Gain and Time Delay Corrections

The HeliUM model was updated using a simple gain and time delay on each of the inputs (Refs. 5 and 7). The corrections are computed by identifying a gain and time delay for the inverse of the error response:

$$\frac{1}{E_{HeliUM,ID}} = \frac{G_{ID}}{G_{HeliUM}} \approx k e^{-s\tau} \quad (7)$$

where $E_{HeliUM,ID}$ is the error response between HeliUM and the ID model, G_{ID} is the bare airframe frequency response of the ID model, G_{HeliUM} and is the bare airframe frequency response of HeliUM. The inverse of the error response is the ideal model correction, which is approximated with an identified gain k and time delay τ corrections. If the ID and HeliUM model responses were identical, than the error response and corrections would both be precisely $k = 1$ with $\tau = 0$ (0 dB magnitude and 0 deg phase). The corrections are computed for each control and the corresponding primary response: a_z/Col , $q/(Symm Lon)$, p/DCP , $p/(Lat Cyclic)$, $r/(Diff Lon)$, and $p/(Lat Mixer)$. The corrections can then easily be applied directly on the control effector signals themselves; corrections are applied to the inputs to the HeliUM model and the HeliUM model itself is unchanged. Corrections to the inputs are applied as follows:

$$u_{updated}(t) = \begin{cases} k_1 u_1(t - \tau_1) \\ \vdots \\ k_n u_n(t - \tau_n) \end{cases} \quad (8)$$

$$\dot{x} = f(x, u_{updated}; t) \quad (9)$$

As the practical implementation does not actually affect the HeliUM bare-airframe model (the equations of motion themselves are unchanged between Eqns. 6 and 9), it is convenient to understand the equivalent net effects using the linear model. The net effects of the gain and delay corrections analyzed by updating the control matrix and input delay vector:

$$B_{updated} = [B_1 k_1 \dots B_n k_n] \quad (10)$$

$$\dot{x} = Ax + B_{updated} \begin{Bmatrix} u_1(t - \tau_1) \\ \vdots \\ u_n(t - \tau_n) \end{Bmatrix} \quad (11)$$

To reiterate, the updated linear models are computed herein for analysis of the net effects of the updates. In practice, the updates are implemented via the nonlinear simulation model inputs themselves as shown in Eqns. 8 and 9.

One important note is that due to the redundancy in the lateral controls, the updated symmetric lateral cyclic control derivatives can be back-computed from DCP and Lat Mixer control derivatives to enforce the known mixing constraint and leverage the derivatives which come from higher quality frequency responses (*p*/DCP and *p*/Lat Mixer). The Symm Lat derivatives are computed as follows:

$$B_{Lat\ Cyclic} = \frac{1}{MR_{Lat\ Cyclic}} [B_{Lat\ Mixer} - MR_{DCP} B_{DCP}] \quad (12)$$

where $MR_{Lat\ Cyclic}$ is the mixing ratio for Lat Cyclic and MR_{DCP} is the mixing ratio for DCP. While the control derivatives for Lat Cyclic are back-calculated, the time delay correction is directly obtained from the *p*/(Lat Cyclic) inverse error response.

Force and Moment Increment and Time Delay Corrections

The HeliUM model was alternately updated by adding force and moment increments (Ref. 7) applied to the nonlinear model itself. This method is sometimes referred to as a “renovation” method, and the updated model is referred to as a “renovated” model.

Deficiencies in the HeliUM model can be analyzed by comparing the HeliUM linear model stability and control derivatives to the identified state space model. To do this, the HeliUM model is first converted to be of the same form as the 6DOF identified state space model. The HeliUM linear model includes the standard 6DOF rigid body states in addition to higher order rotor and inflow states:

$$x = \begin{Bmatrix} x_{RB} \\ x_{HO} \end{Bmatrix} \quad (13)$$

The higher order states are residualized (Ref. 10) using a standard steady-state approximation (assume higher order dynamics are significantly faster than rigid body dynamics)

$$\dot{x}_{HO} = 0 \quad (14)$$

which allows the steady state effects of the higher order states to be subsumed into the remaining 6DOF rigid body dynamics:

$$x_{6DOF} = \{x_{RB}\} \quad (15)$$

This residualization process allows the remaining state-space structure to maintain correspondence with the rigid body dynamics.

With reduced 6DOF HeliUM model now in the same form as the identified 6DOF model, the increments to the stability and control derivatives can be directly computed as the difference between the HeliUM and identified derivatives:

$$A_{Inc} = A_{ID} - A_{HeliUM\ 6DOF} \quad (16)$$

$$B_{Inc} = B_{ID} - B_{HeliUM\ 6DOF} \quad (17)$$

The increments can then be added directly to the rigid body equations of motion in the HeliUM nonlinear model:

$$\begin{Bmatrix} \dot{x}_{RB} \\ \dot{x}_{HO} \end{Bmatrix} = \begin{Bmatrix} f_{RB}(x_{RB}, x_{HO}, u, t) + [A_{Inc}]x_{RB} + [B_{Inc}]u \\ f_{HO}(x_{RB}, x_{HO}, u, t) \end{Bmatrix} \quad (18)$$

The updated HeliUM model can then be relinearized to check whether the increments produce the intended forces and moments. The relinearized updated HeliUM model should have the form:

$$\begin{Bmatrix} \dot{x}_{RB} \\ \dot{x}_{HO} \end{Bmatrix} \approx \begin{bmatrix} A_{11} + A_{Inc} & A_{12} \\ A_{21} & A_{22} \end{bmatrix} \begin{Bmatrix} x_{RB} \\ x_{HO} \end{Bmatrix} + \begin{bmatrix} B_1 + B_{Inc} \\ B_2 \end{bmatrix} \{u\} \quad (19)$$

where the increments act only on the rigid body equations of motion. The relinearized updated HeliUM model can then be reduced down to the 6DOF form to check if the updated 6DOF stability and control derivatives match the ID model.

In most cases, the updated HeliUM 6DOF stability and control derivatives will be closer to, but not exactly match the desired updated model which is the ID model. This is thought to be due to the practical implementations of the physics-based nonlinear HeliUM model where components are numerically computed including linearization. To alleviate this, the 6DOF force and moment increments themselves are iteratively updated based on the residual differences between the desired increments (differences in derivatives) and the resulting increments. The increment adjustments are computed as follows (note: the 6DOF notation is dropped for convenience):

$$[k_{A_n}]_{i,j} = \frac{[A_{Desired}]_{i,j} - [A_{HeliUM_0}]_{i,j}}{[A_{HeliUM_n}]_{i,j} - [A_{HeliUM_0}]_{i,j}} \quad (20)$$

where $[k_{A_n}]_{i,j}$ is the increment adjustment factor for the n^{th} iteration of the 6DOF stability matrix A element i,j ; $[A_{HeliUM_n}]_{i,j}$ is the i,j 6DOF stability derivative for HeliUM at the n^{th} iteration. The increment adjustment factor is applied to the increment as:

$$[A_{Inc_{n+1}}]_{i,j} = [k_{A_n}]_{i,j} [A_{Inc_n}]_{i,j} \quad (21)$$

The increment adjustment factors are computed for all stability and control derivatives. Without the additional increment adjustment factors, some of the resulting increments were off by as much as 30% compared to the desired ideal increments. It was found that updating the increments twice (i.e. $n = 1,2$) produced linear HeliUM models which were sufficiently close to the desired updated model.

It should be noted that the increments are only computed for and applied to stability and control derivative terms themselves in the force and moment equations of motion. Increments are not computed for or applied to gravity terms or kinematic constraints. The notation used in the equations presented herein is simplified for brevity.

Comparisons of the various stability and control derivatives can be visually depicted with a bar chart. The control derivatives for DCP can be seen in Figure 17 for the ID model and each of the three HeliUM models [original, updated gain and time delay ($k&\tau$), updated with force and moment increments (FM& τ)]. The roll moment control derivative L_δ is of course the primary driver for the roll rate response. As the L_δ derivatives are all close (updated models are the same as ID model, original HeliUM is still fairly close), the resulting roll rate primary responses to DCP for each model are also close.

The control derivatives for Lat Cyclic can be seen in Figure 18 for the ID model and each of the three HeliUM models. Again, the roll moment control derivative L_δ is the primary driver for the roll rate response. Also, as the L_δ derivatives are all close, the resulting roll rate primary responses to Lat Cyclic for each model are close. However, the original HeliUM lateral force control derivative Y_δ is very large compared to the ID model, resulting in a large discrepancy for lateral accelerometer response a_y /Lat Cyclic. This is slightly improved for the gain and time delay update model, but it is greatly improved for the force and moment increment update model as that individual derivative can be updated independently of the others.

The data provided by the JIO method allow for the computation of the force and moment increments for the control derivatives associated with DCP and Lat Cyclic. Without the JIO method, responses for DCP and Lat Cyclic cannot be precisely separated and thus the associated increments cannot be precisely calculated. This capability is the primary benefit of using the JIO method with respect to the work presented herein.

The control derivatives for Diff Lon can be seen in Figure 19 for the ID model and each of the three HeliUM models. The yaw moment control derivative N_δ is of course the primary driver for the yaw rate primary response r /Diff Lon. As the Y_δ derivatives are all close, the resulting roll rate primary

responses to Diff Lon for each model are also close. However, the original HeliUM roll moment control derivative L_δ is small and of the opposite sign compared to the ID model, resulting in very poor agreement for the secondary response p /Diff Lon. The gain and time delay update model does just as poorly as the original HeliUM model. However, control derivative L_δ is greatly improved for the force and moment increment update model as that individual derivative can be updated independently of the others.

Overall, the both model update methods are effective in improving agreement between updated HeliUM models and the identified model. The primary control derivatives for the gain and time delay update model match the identified model. For the force and moment increment update model, all control derivatives (primary and secondary) closely track the identified model.

Lastly, the stability derivatives for the roll rate response can be seen in Figure 20 for the ID model and each of the three HeliUM models. The roll damping derivative L_p , along with lateral speed damping Y_v and lateral speed stability L_v are the primary drivers for the lateral hovering cubic characteristics (Ref. 11). The roll damping term is significantly under predicted (in terms of magnitude) by the original HeliUM model; the force and moment increments are able to correct this roll damping derivative accordingly. Similar errors and increments for the HeliUM model are observed and applied for all stability derivatives. The gain and delay corrections are of course unable to affect the stability derivatives.

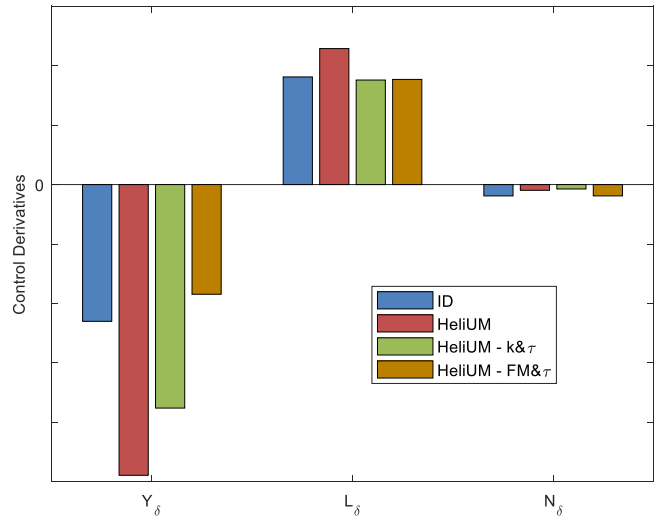


Figure 17. DCP Control Derivatives for HeliUM Updated Models.

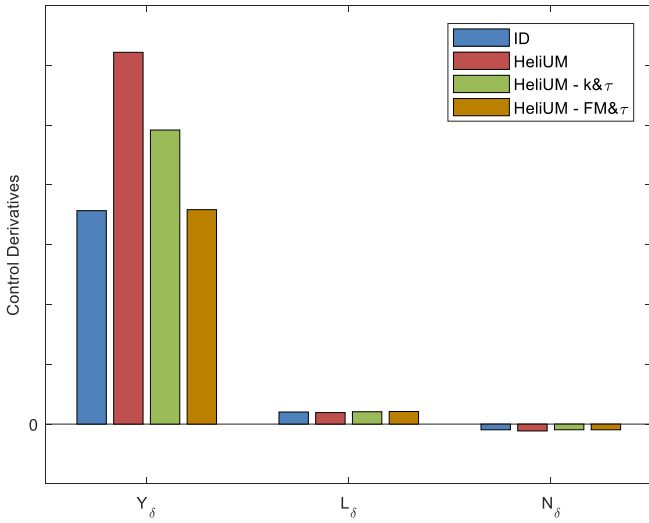


Figure 18. Lat Cyclic Control Derivatives for HeliUM Updated Models.

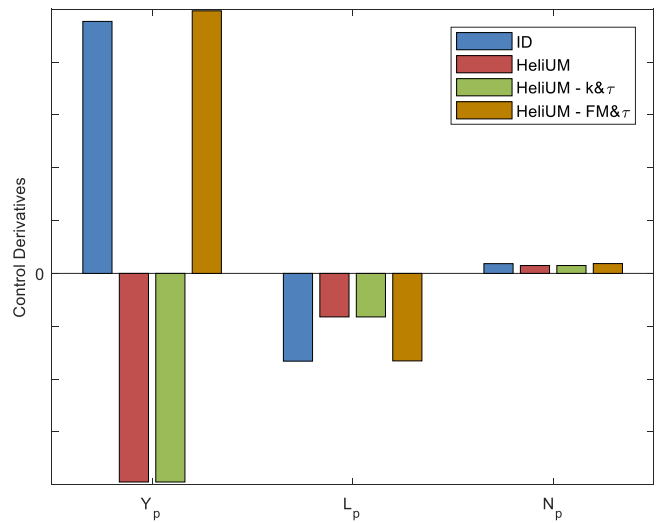


Figure 20. Roll Rate Stability Derivatives for HeliUM Updated Models.

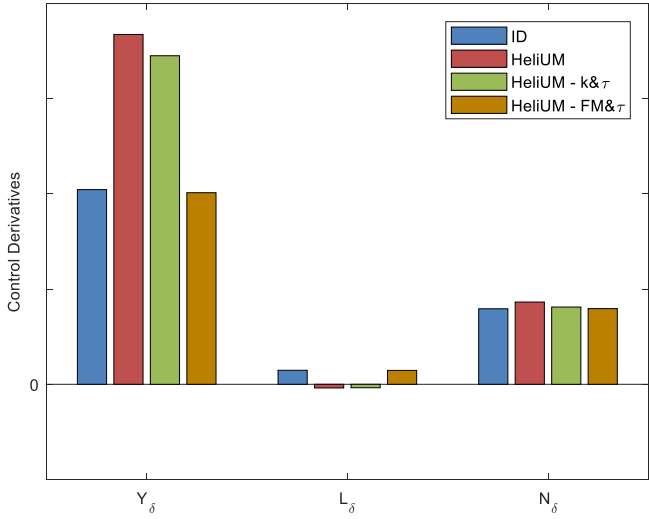


Figure 19. Diff Lon Control Derivatives for HeliUM Updated Models.

In addition to the force and moment increments, time delay corrections are also computed and applied. The time delay corrections are identified based on the inverse of the error response between the HeliUM model with force and moment corrections and the flight test responses:

$$\frac{1}{E_{HeliUM,FT}} = \frac{G_{FT}}{G_{HeliUM}} \approx e^{-s\tau} \quad (22)$$

where $E_{HeliUM,FT}$ is the error response between HeliUM and the flight test response, G_{FT} is the bare airframe frequency response from flight test, G_{HeliUM} and is the bare airframe frequency response of HeliUM. The inverse error response is the ideal correction which is approximated with a time delay τ correction. The delay corrections are computed for all output/control pairs which were sufficiently identified from the flight test data. This creates a full matrix of time delay corrections. While it is possible to implement the full time delay matrix for all output/control pairs, it is more practical to instead appropriate delays only to output (τ_y) and control (τ_u) delays.

The approach used is to first appropriate control input delays based on the primary on-axis responses (i.e. p /DCP, p /Lat Cyclic, etc), and appropriate remaining residual delays to sensor/output delays where possible. This creates delays which are easily implemented in simulation, but not all of the updated model phase responses are closely correlated to the flight test data. The resulting relinearized models include the input and output delays are of the form:

$$\dot{x} = A_{updated}x + B_{updated} \begin{Bmatrix} u_1(t - \tau_{u,1}) \\ \vdots \\ u_n(t - \tau_{u,n}) \end{Bmatrix} \quad (23)$$

$$\begin{Bmatrix} y_1(t + \tau_{y,1}) \\ \vdots \\ y_m(t + \tau_{y,m}) \end{Bmatrix} = C_{updated}x + D_{updated} \begin{Bmatrix} u_1(t - \tau_{u,1}) \\ \vdots \\ u_n(t - \tau_{u,n}) \end{Bmatrix} \quad (24)$$

It should be noted that the output equation matrices $C_{updated}$ and $D_{updated}$ are not directly updated based on the force and moment increments. Recall that they are based on kinematic constraints which relate the states and state derivatives to the measured outputs (i.e., accelerometer measurement is a function of body axis acceleration and attitude) which are invariant with respect to the update methods with the exception of the output delay:

$$y(t + \tau_y) = H_0x + H_1\dot{x} \quad (25)$$

The state equation is substituted for the state derivatives in the output equation resulting in the outputs being a function of states and controls, and thus indirectly being updated by the new force and moment increments.

Updated Model Fidelity

Each of the HeliUM models [original, updated gain and time delay ($k\&\tau$), updated with force and moment increments (FM $\&\tau$)] are compared with the flight test frequency responses as well as the identified state space model. The identified state space model provides a good baseline for comparison with the HeliUM models, as it is the most accurate kinematically consistent 6DOF model in terms of correlating with the flight test data.

The pitch rate response q to Symm Lon is shown in Figure 21. The original HeliUM model already correlates well with the flight test data for mid and high frequency, however there is poor agreement with flight test data for low frequency ($J = 462.3$), particularly with respect to the peak magnitude associated with the hovering cubic. The gain and delay corrections have minimal improvement on HeliUM accuracy, as the corrections primarily align mid and high frequency ranges which are already in good agreement with the flight test data; the gain and delay corrections are unable to change the low-mid frequency characteristics associated with the system dynamics such as the hovering cubic. The force and moment corrections significantly improve the HeliUM correlation with flight test data ($J = 190.0$). This a result of the force and moment corrections being able to change low-mid frequency characteristics to align with the identified model; e.g. the peak in magnitude in q /Symm Lon associated with the longitudinal hovering cubic peak closely matches with the identified model characteristics (peak magnitude, phase, and frequency).

The roll rate response p to DCP is shown in Figure 22, and the yaw rate response r to DCP is shown in Figure 23. The original HeliUM model already correlates well with the flight test data for p /DCP ($J = 70.5$), however there is poor agreement with flight test data for r /DCP ($J = 317.8$). The gain

and delay corrections improve the agreement with HeliUM for the primary response p /DCP as good as the identified model ($J = 18.5$), but actually make the correlation for the secondary response r /DCP worse ($J = 621.8$). This is due to the gain and delay corrections only being able to act on DCP itself rather than actually updating on the bare-airframe model directly.

The force and moment corrections improve the HeliUM correlation with flight test data for both p /DCP ($J = 5.2$) and r /DCP ($J = 58.7$). This improvement in both responses is primarily due to the updated control effectiveness for DCP with respect to individual forces and moments; i.e., the resulting re-linearized Y_{DCP} , L_{DCP} , and N_{DCP} are all updated independently to match the identified results as shown in Fig. 17.

The lateral accelerometer response to Diff Lon is shown in Figure 24. The identified state space model has an acceptable cost function $J = 64 < 100$ and correlates well with the flight test data. The HeliUM original model is in poor agreement with the flight test result with large discrepancies in magnitude and phase ($J = 858$). The original HeliUM model is flat at low-mid frequency, while the identified state space model has a dipole at low-mid frequency; this difference is likely due to discrepancies in the accelerometer measurement location. At mid-high frequency, the original HeliUM phase slope does not agree with the flight test data; these mid-high frequency discrepancies are attributed to the low fidelity approximations of the sensor/measurement system with a simple delay, approximations which are unable to capture all of the complexities of the true sensor dynamics. The force and moment increments are able to improve agreement with the flight test data in terms of magnitude, however the characteristic of the phase response is still not captured correctly.

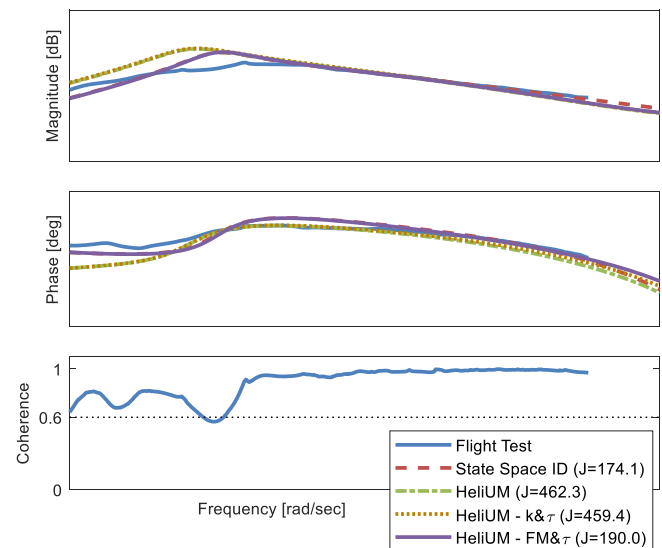


Figure 21. V-280 Pitch Rate Response to Symm Lon for HeliUM Updated Models.

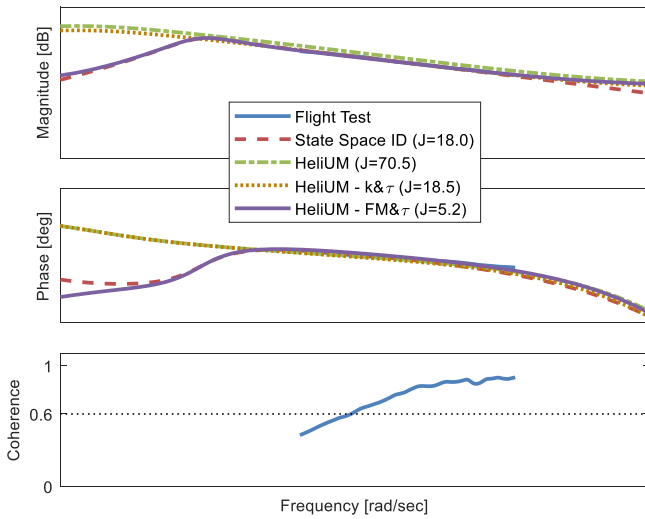


Figure 22. V-280 Roll Rate Response to DCP for HeliUM Updated Models.

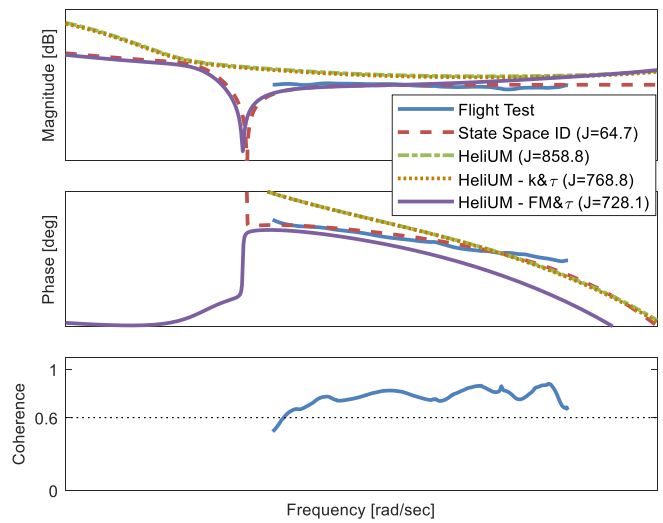


Figure 24. Lateral Accelerometer Response to Diff Lon for HeliUM Updated Models.

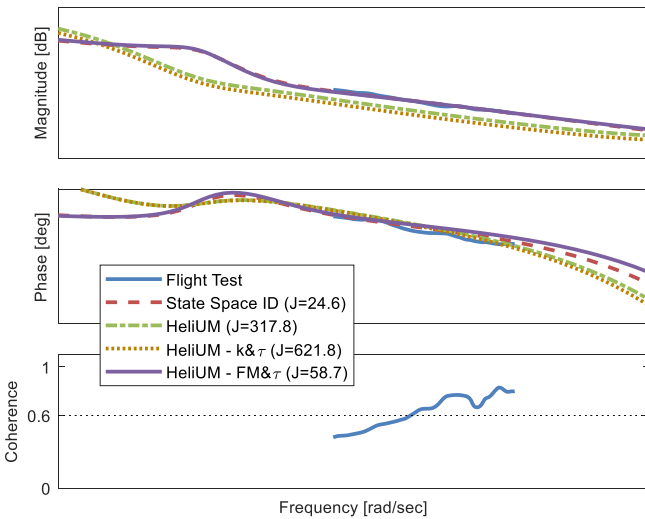


Figure 23. V-280 Yaw Rate Response to DCP for HeliUM Updated Models.

The model fidelity assessment can also be performed by examining the error responses between the flight test results and the individual models. The error responses can be computed by dividing model response with the flight test response:

$$E_{Model,FT} = \frac{G_{Model}}{G_{FT}} \quad (26)$$

where $E_{Model,FT}$ is the error response between the model and the flight test response, G_{FT} is the bare airframe frequency response from flight test, G_{Model} and is the bare airframe frequency response of the model. An error response value of 1 (0 dB error and 0 deg phase error) would indicate the model perfectly correlates to flight test data. One benefit of examining the error response is that the models can be validated at a specific frequency by comparison with an acceptability bound. Examples of acceptability bounds (Ref. 7) include the Maximum Unnoticeable Added Dynamics (MUAD) (Refs. 5 and 12) and the Allowable Error Envelopes (AEE) (Ref. 13).

The error response for r /Diff Lon is shown in Figure 25. Each model is within the acceptable boundary through the entire frequency range, thus it is unsurprising that the associated cost functions are all also acceptable with $J < 100$.

The error response for p /Lat Mixer is shown in Figure 26. Although each model has an acceptable cost function $J < 100$. The original HeliUM model is somewhat close to the acceptable cost guideline with $J = 88.2 < 100$ and marginally exceeds the upper acceptable error bound through most of the available frequency range. Thus, the original HeliUM p /Lat Mixer response is considered borderline acceptable. This illustrates that the acceptable error bounds and acceptable cost guideline ($J < 100$) are aligned, yet also highlights the need to look at multiple metrics when assessing model fidelity.

Lastly, the error response for q /Symm Lon is shown in Figure 27. All 3 of the models have high cost functions $J \gg 100$, however all of the models actually fall within the acceptable boundary for a significant portion of the frequency range. In fact, all of the models are within the acceptable bounds for the mid frequency range which is the most critical frequency range where the acceptable boundaries are the tightest (corresponding to where feedback and piloted action is most anticipated). Thus, while none of the models meet the specified acceptability criteria, it is primarily due to errors at low-to-mid frequencies which are less critical.

The overall model fidelity is presented in Table 3 which presents all of the cost functions for individual frequency responses as well as the average. Costs functions are presented for the identified model as well as each of the three HeliUM models.

The cost of the identified model is acceptable with an average cost function $J = 94 < 100$. The original HeliUM model with no corrections correlates well with flight test data for primary responses, but has poor agreement with flight test data for many of the secondary responses.

The HeliUM model with gain and time delay corrections further improves the primary responses, however in many cases the secondary responses are actually worsened. Overall the HeliUM model with gain and time delay corrections provides a slight improvement in the average cost function and model fidelity.

The HeliUM model with force and moment increment corrections overall does well coming closest to the identification results with the best average cost function and model fidelity of the three HeliUM models. The response with higher cost functions are primarily due to discrepancies in phase, which are attributed to the low fidelity approximations of the sensor/measurement system (approximations which are unable to capture all of the complexities of the true sensor dynamics).

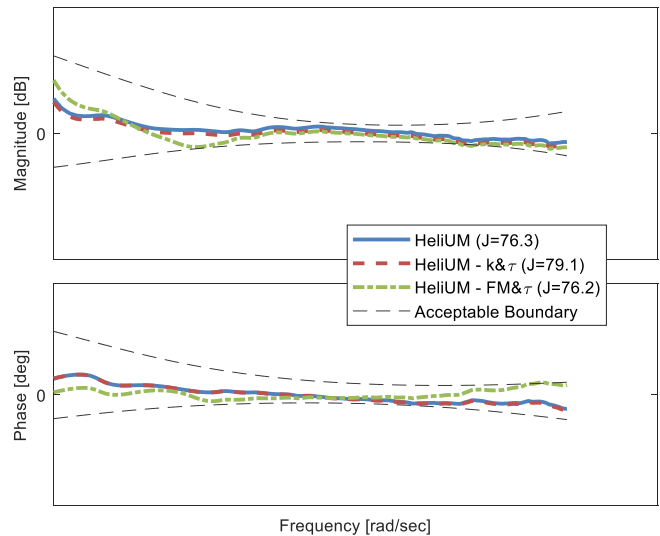


Figure 25. Error Response Yaw Rate to Diff Lon.

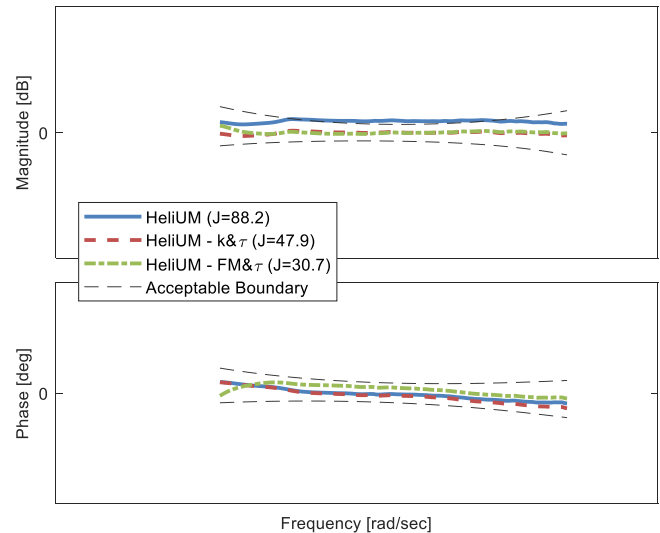


Figure 26. Error Response Roll Rate to Lat Mixer.

Table 3. Cost Functions for Model Updates

Response	ID	HeliUM	HeliUM	HeliUM
		No Corrections	k & τ Corrections	FM & τ Corrections
a_z /Coll	56	117	75	85
q /Symm Lon	174	462	459	190
a_x /Symm Lon	29	285	326	42
a_z /Symm Lon	116	7053	6571	254
udot/Symm Lon	315	1544	1573	317
p /DCP	18	71	18	5
r /DCP	25	318	622	59
p /Lat Cyclic	199	323	183	140
r /Lat Cyclic	101	227	134	42
a_y /Lat Cyclic	75	479	329	115
vdot/Lat Cyclic	61	873	600	107
p /Diff Lont	151	1660	1762	54
r /Diff Lon	73	76	79	76
a_y /Diff Lon	64	859	769	728
vdot/Diff Lon	114	854	757	1161
p /Lat Mixer	57	88	48	31
r /Lat Mixer	62	55	169	38
a_y /Lat Mixer	46	821	583	54
vdot/Lat Mixer	51	192	259	34
Average	94	861	806	187

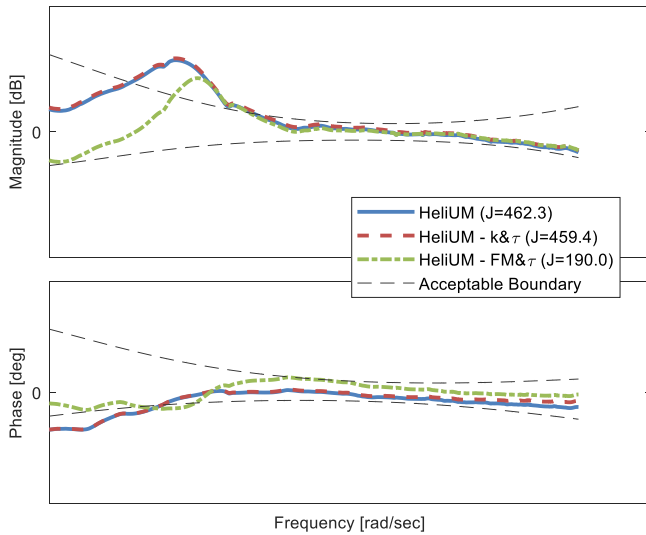


Figure 27. Error Response Pitch Rate to Symm Lon.

CONCLUSIONS

Flight test data from the Bell V-280 Valor in hover was used to extract frequency responses and identify a state space model. The identification results were used to validate physics based and Froude scaled models. The government physics based model was then updated using two different techniques to improve model correlation with flight test data. The results of the analysis support the following conclusions:

1. The Direct method for frequency response identification provides the best overall quality, however the JIO method allows separation of responses with respect to individual effectors. A combination of both methods allows sufficient data for a full state space identification with respect to individual control effectors.
2. Froude scale models work well for quickly estimating primary responses.
3. Uncorrected physics based models work well for predicting primary responses and some secondary responses.
4. Gain and time delay corrections improve model correlations with flight test data for primary responses.

5. Force and moment increment corrections greatly improve model correlations with flight test data for primary and secondary responses.
6. Realized force and moment increments after implementation and re-linearization may differ from the desired increments. An iterative method is effective for calculating and adjusting increments such that the re-linearized model closely tracks the desired model.

ACKNOWLEDGMENTS

The success of this joint project is due to the efforts and support of many contributors beyond the authors of this paper. In particular, the authors would like to thank the Bell V-280 team and the DEVCOM AvMC JMR-TD and FVL teams for support throughout the V-280 development.

REFERENCES

1. Ivler, C. M., Rowe, E. S., Martin, J., Lopez, M. J. S., and Tischler, M. B., "System Identification Guidance for Multirotor Aircraft: Dynamic Scaling and Test Techniques," presented at the AHS International 75th Annual Forum & Technology Display, Philadelphia, PA, May 13-16, 2019.
2. Padfield, G. G., *Helicopter Flight Dynamics including a treatment of Tiltrotor Aircraft Third Edition*, Wiley, 2018, pp. 22-24 and Chapter 3.
3. Berrigan, C., Lopez, M. J. S., Ruckel, P., and Prasad, J. V. R., "Bell V-280 System Identification: Application of JIO Methodology for Hover Model Identification," presented at the Rotorcraft Handling Qualities Technical Meeting, Huntsville, Alabama, USA, February 19-20, 2020.
4. Berrigan, C., Lopez, M. J. S., Ruckel, P., and Prasad, J. V. R., "Bell V-280 System Identification and Model Validation with Flight Test Data using the Joint Input-Output Method," presented at the Vertical Flight Society's 76th Annual Forum & Technology Display, Virtual, October 6-8, 2020.
5. Tischler, M. B. and Remple, R. K., *Aircraft and Rotorcraft System Identification: Engineering Methods and Flight Test Examples Second Edition*, AIAA 2012.
6. Berger, T., Tischler M. B., Knapp, M. E., and Lopez, M. S., "Identification of Multi-Input Systems in the Presence of Highly correlated Inputs," presented at the Atmospheric Flight Mechanics Conference at AIAA SciTech, San Diego, CA, January 7-11, 2019.
7. Tischler, M. B., White, M. D., Cameron, N., D'Agosto, S., Greiser, S., Gubbels, A., Guner, F., He, C., Horn, J., Hui, K., Jones, M., Juhasz, O., Lee, O., Lehmann, R., Miller, D., Myrand-Lapierre, V., Nadeau-Beaulieu, M., Nadell, S., Padfield, G., Pavel, M., Prasad, J., Ragazzi, A., Richard, S., Scepanovic, P., Seher-Weiß, S., Soong, J., Stroosma, O., Taghizad, A., Tobias, E., Xin, H., and Yavrucuk, I. (2021), "Rotorcraft Flight Simulation Model Fidelity Improvement and Assessment," NATO STO AVT-296 Technical Report.
8. Berger, T., Lopez, M. J. S., Wagner, A. M., Tischler, M. B., "Guidelines for System Identification of Multirotor Vehicles with Highly Correlated Inputs" presented at the Vertical Flight Society's 76th Annual Forum & Technology Display, Virtual, October 6-8, 2020.
9. Celi, R., "HeliUM 2 Flight Dynamics Simulation Model: Development, Technical Concepts, and Applications" presented at the AHS 71st Annual Forum, Virginia Beach, VA, May 5-7, 2015.
10. Kokotovic, P. V., O'Malley Jr., R. E., and Sannuti, P., "Singular perturbations and order reduction in control theory – An overview," *Automatica*, Vol. 12 (2), March 1976, pp. 123-132, doi: 10.1016/0005-1098(76)90076-5.
11. McRuer, D. T., Graham, D., and Ashkenas, I., *Aircraft Dynamics and Automatic Control*, Princeton University Press, Princeton, VA, 1973.
12. Hodgkinson, J. *Aircraft Handling Qualities*, AIAA Education Series, AIAA, Reston, VA, 1998.
13. Mitchell, D. G., Hoh, R. H., He, C., and Strobe, K., "Development of an aeronautical design standard for validation of military helicopter simulators," 62nd Annual Forum of the American Helicopter Society, Phoenix, AZ, 2006.